

Efficient Analysis of Multilayered Dielectric Rods by Equivalent Microwave Network Method

Liangqi Gui¹, Cong Zhou^{1, *}, Xinxin Tian², Fan Yang³, and Yao-Jiang Zhang⁴

Abstract—Multilayered dielectric rods are widely used, and the analysis of their electromagnetic scattering properties is very important in practical design. Based on our former work on the single layer dielectric rod forest, the equivalent microwave network method (EMN) is applied to analyse the concentric and eccentric multilayered dielectric rods in this article. The key step is to obtain the reflection matrix of the multilayered dielectric. Based on the EMN method, the electromagnetic scattering properties of a novel electromagnetic band gap (EBG) structure are calculated. The EBG structure is formed by periodically embedding multilayered dielectric rods into the original dielectric between power/ground planes. The accuracy and efficiency of the EMN method are verified by comparing with the simulation results by the FIT simulator CST. In addition, the EMN method takes about 1 minute to obtain the results, while the simulator takes nearly 20 hours with the same computer.

1. INTRODUCTION

As a typical 2-D electromagnetic (EM) computing problem, scattering by cylindrical structures is widely studied. A great variety of practical scatterers can be modeled as single layer cylindrical rods or multilayered cylindrical rods. One of the most important scattering parameters is the radar cross section (RCS). For a cylinder of infinite length l , the 3-D RCS for normal incidence is related to 2-D scattering width (SW) [1].

Previous investigations that estimate the scattering properties of cylindrical structures exist in the literature. The scattering characteristics of single or multiple cylindrical rods in a nonabsorbent or absorbing medium have been studied in [2–5]. The scattering of oblique incident electromagnetic wave into cylindrical rods array is calculated in [6]. Multilayered eccentric dielectric rods are studied by the indirect mode-matching solution in [7–9]. Rigorous Coupled Wave Analysis (RCWA) algorithm is applied in [10–12] to study EM scattering by multi-eccentric circular or elliptical cylinders. For single layer dielectric rod forest, we have analysed the EM properties in [13, 14], and the equivalent microwave network method (EMN) is applied in the analysis process.

For multilayered rods, the scattering analysis algorithms mentioned above are complex and time-consuming. Based on our former work on single layer rod [13, 14], the EMN method is proposed in this paper to analyze the multilayered rod. Generalized scattering matrix, namely, S -parameters matrix is used to characterize the scattering properties of each interface between different materials. Electromagnetic fields are expressed in terms of cylindrical waves. Then the S -parameters matrix of a multilayered dielectric rod is calculated by microwave network method, and the reflection matrix of multilayered rod is deduced from S -parameters matrix. By loading the reflection matrix to the

Received 8 November 2016, Accepted 30 December 2016, Scheduled 15 January 2017

* Corresponding author: Cong Zhou (zhoucong@hust.edu.cn).

¹ The Science and Technology on Multi-Spectral Information Processing Laboratory, School of Electronic Information and Communications, Huazhong University of Science and Technology, Wuhan 430074, China. ² School of Physics and Optoelectronic Engineering, Guangdong University of Technology, Guangzhou, Guangdong Province 510006, P. R. China. ³ The Space Science Institute from Macaw University of Science and Technology, Macaw 00853, China. ⁴ Huawei Technologies Co., Ltd., Shenzhen 518129, China.

radial scattering matrix of parallel plate pair, the performance of a novel EBG structure can be easily calculated.

The proposed method converts complex scattering problems into microwave network issues. It keeps the accuracy of field matching method and simplifies the analysis procedure. Furthermore, it possesses a clear physical conception and provides convenience for analysing multiple rods and multilayered cylindrical rods.

This paper is organized as follows. In Section 2, the geometries and EM models of concentric and eccentric multilayered rods are presented. In Section 3, the scattering parameters of multilayered rods array are derived. In Section 4, several examples are provided to demonstrate the accuracy of EMN by comparing with the full-wave solver CST.

2. RADIAL SCATTERING MATRIX FOR MULTILAYERED DIELECTRIC RODS

2.1. Scattering Matrix of Two Adjacent Layers

The geometric drawing of a m -layer dielectric rod is shown in Fig. 1. The relative permittivity and relative permeability of each layer are $\varepsilon_{r0}, \varepsilon_{r1}, \dots, \varepsilon_{rm}$ and $\mu_{r0}, \mu_{r1}, \dots, \mu_{rm}$. The subscript 0 means the outer space and the subscript m means the innermost layer. The cylindrical coordinate is set up at the center of the rod. A plane wave travels in the $+x$ direction. According to [15], the incident fields and scattered fields can be expressed by Bessel and Hankel function, respectively. For the i th and $(i+1)$ th layer, the electric and magnetic field can be written as

$$\mathbf{E}_i = \mathbf{a}_z \sum_{n=-N_i}^{N_i} \left[\mathbf{a}_n^i \mathbf{J}_n(\mathbf{k}_i \rho) + \mathbf{b}_n^i \mathbf{H}_n^{(2)}(\mathbf{k}_i \rho) \right] \mathbf{e}^{jn\varphi} \quad (1)$$

$$\mathbf{E}_{i+1} = \mathbf{a}_z \sum_{n=-N_{i+1}}^{N_{i+1}} \left[\mathbf{a}_n^{i+1} \mathbf{J}_n(\mathbf{k}_{i+1} \rho) + \mathbf{b}_n^{i+1} \mathbf{H}_n^{(2)}(\mathbf{k}_{i+1} \rho) \right] \mathbf{e}^{jn\varphi} \quad (2)$$

$$\mathbf{H}_i^\varphi = \mathbf{a}_\varphi \frac{\mathbf{k}_i}{\mu_0 \mu_{ri}} \sum_{n=-N_i}^{N_i} \left[\mathbf{a}_n^i \mathbf{J}'_n(\mathbf{k}_i \rho) + \mathbf{b}_n^i \mathbf{H}_n^{(2)'}(\mathbf{k}_i \rho) \right] \mathbf{e}^{jn\varphi} \quad (3)$$

$$\mathbf{H}_{i+1}^\varphi = \mathbf{a}_\varphi \frac{\mathbf{k}_{i+1}}{\mu_0 \mu_{r(i+1)}} \sum_{n=-N_{i+1}}^{N_{i+1}} \left[\mathbf{a}_n^{i+1} \mathbf{J}'_n(\mathbf{k}_{i+1} \rho) + \mathbf{b}_n^{i+1} \mathbf{H}_n^{(2)'}(\mathbf{k}_{i+1} \rho) \right] \mathbf{e}^{jn\varphi} \quad (4)$$

where $k_i = k_0 \sqrt{\varepsilon_{ri} \mu_{ri}}$, $k_{i+1} = k_0 \sqrt{\varepsilon_{r(i+1)} \mu_{r(i+1)}}$. μ_0 is the permeability of free space and k_0 is the wave number in free space. a_n^i and b_n^i represent the unknown amplitude coefficients of incident fields and

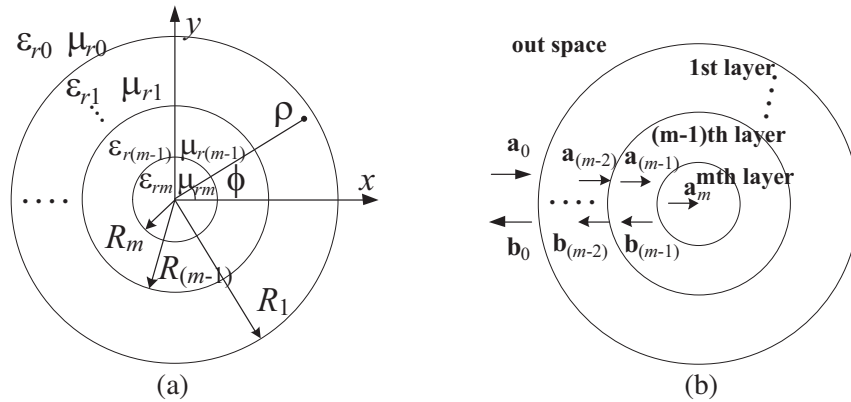


Figure 1. Multilayered dielectric rod. (a) Radii and relative permittivity and permeability notations. (b) The incident and scattered field coefficients vector in each layer.

scattered fields respectively in the i th layer. The truncation number N_i and N_{i+1} could be different for each layer and they are set as a fixed integer N in this article. To facilitate further discussions, the expansion coefficients a_n^i , b_n^i , a_n^{i+1} and b_n^{i+1} are arranged into vectors in the following sequences as shown in Fig. 1.

$$\mathbf{a}_i = [a_{-N}^i \quad a_{-N+1}^i \quad \cdots \quad a_N^i]^T \quad (5)$$

$$\mathbf{b}_i = [b_{-N}^i \quad b_{-N+1}^i \quad \cdots \quad b_N^i]^T \quad (6)$$

$$\mathbf{a}_{i+1} = [a_{-N}^{i+1} \quad a_{-N+1}^{i+1} \quad \cdots \quad a_N^{i+1}]^T \quad (7)$$

$$\mathbf{b}_{i+1} = [b_{-N}^{i+1} \quad b_{-N+1}^{i+1} \quad \cdots \quad b_N^{i+1}]^T \quad (8)$$

Assuming that the interface between the i th and $(i+1)$ th layer is a two-port microwave device, the four expansion coefficient vectors can be related by a generalized scattering matrix \mathbf{S}_i :

$$\begin{bmatrix} \mathbf{b}_i \\ \mathbf{a}_{i+1} \end{bmatrix} = [\mathbf{S}_i] \begin{bmatrix} \mathbf{a}_i \\ \mathbf{b}_{i+1} \end{bmatrix} \quad (9)$$

The generalized scattering matrix can be expressed as following submatrices:

$$[\mathbf{S}_i] = \begin{bmatrix} \mathbf{S}_{11,i} & \mathbf{S}_{12,i} \\ \mathbf{S}_{21,i} & \mathbf{S}_{22,i} \end{bmatrix} \quad (10)$$

The four submatrices \mathbf{S}_{**i} in \mathbf{S}_i are $(2N+1) \times (2N+1)$ diagonal matrices. According to the boundary condition of dielectric rod in cylindrical coordinate:

$$\mathbf{E}_i = \mathbf{E}_{i+1} \quad (11)$$

$$\mathbf{H}_i^\varphi = \mathbf{H}_{i+1}^\varphi \quad (12)$$

Eqs. (1)–(4) can be written as

$$a_n^i J_n(k_i R_{i+1}) + b_n^i H_n^{(2)}(k_i R_{i+1}) = a_n^{i+1} J_n(k_{i+1} R_{i+1}) + b_n^{i+1} H_n^{(2)}(k_{i+1} R_{i+1}) \quad (13)$$

$$\frac{k_1}{\mu_{r1}} [a_n^i J_n'(k_i R_{i+1}) + b_n^i H_n^{(2)'}(k_i R_{i+1})] = \frac{k_2}{\mu_{r2}} [a_n^{i+1} J_n'(k_{i+1} R_{i+1}) + b_n^{i+1} H_n^{(2)'}(k_{i+1} R_{i+1})] \quad (14)$$

Substituting Eqs. (13) and (14) into Eqs. (9) and (10) leads to

$$\mathbf{S}_{11,i} = \text{diag} \left\{ \frac{k_i \mu_{r(i+1)} J_n'(k_i R_{i+1}) * J_n(k_{i+1} R_{i+1}) - J_n(k_i R_{i+1}) * k_{i+1} \mu_{ri} J_n'(k_{i+1} R_{i+1})}{H_n^{(2)}(k_i R_{i+1}) * k_{i+1} \mu_{ri} J_n'(k_{i+1} R_{i+1}) - k_i \mu_{r(i+1)} H_n^{(2)'}(k_i R_{i+1}) * J_n(k_{i+1} R_{i+1})} \right\} \quad (15)$$

$$\mathbf{S}_{12,i} = \text{diag} \left\{ \frac{H_n^{(2)}(k_{i+1} R_{i+1}) * k_{i+1} \mu_{ri} J_n'(k_{i+1} R_{i+1}) - k_{i+1} \mu_{ri} H_n^{(2)'}(k_{i+1} R_{i+1}) * J_n(k_{i+1} R_{i+1})}{H_n^{(2)}(k_i R_{i+1}) * k_{i+1} \mu_{ri} J_n'(k_{i+1} R_{i+1}) - k_i \mu_{r(i+1)} H_n^{(2)'}(k_i R_{i+1}) * J_n(k_{i+1} R_{i+1})} \right\} \quad (16)$$

$$\mathbf{S}_{21,i} = \text{diag} \left\{ \frac{k_i \mu_{r(i+1)} J_n'(k_i R_{i+1}) * H_n^{(2)}(k_i R_{i+1}) - J_n(k_i R_{i+1}) * k_i \mu_{r(i+1)} H_n^{(2)'}(k_i R_{i+1})}{H_n^{(2)}(k_i R_{i+1}) * k_{i+1} \mu_{ri} J_n'(k_{i+1} R_{i+1}) - k_i \mu_{r(i+1)} H_n^{(2)'}(k_i R_{i+1}) * J_n(k_{i+1} R_{i+1})} \right\} \quad (17)$$

$$\mathbf{S}_{22,i} = \text{diag} \left\{ \frac{H_n^{(2)}(k_{i+1} R_{i+1}) * k_i \mu_{r(i+1)} H_n^{(2)'}(k_i R_{i+1}) - k_{i+1} \mu_{ri} H_n^{(2)'}(k_{i+1} R_{i+1}) * H_n^{(2)'}(k_i R_{i+1})}{H_n^{(2)}(k_i R_{i+1}) * k_{i+1} \mu_{ri} J_n'(k_{i+1} R_{i+1}) - k_i \mu_{r(i+1)} H_n^{(2)'}(k_i R_{i+1}) * J_n(k_{i+1} R_{i+1})} \right\} \quad (18)$$

2.2. Reflection Coefficient of a Single-Layer Rod

For the innermost layer of the multilayered rod, two types are considered as shown in Fig. 2: the PEC rod and the dielectric rod.

For a PEC rod, there are no electric or magnetic fields inside the conductor. The boundary condition is

$$E_m(\rho = R_m, 0 \leq \varphi \leq 2\pi) = 0 \quad (19)$$

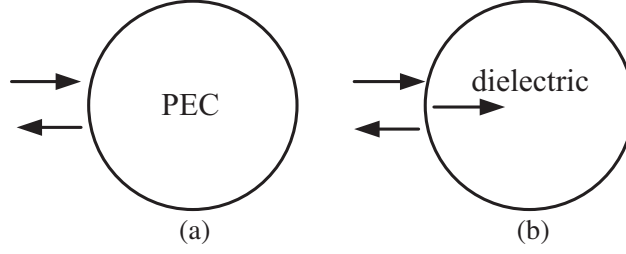


Figure 2. Innermost layer: (a) PEC, (b) dielectric.

From Eq. (1), Eq. (19) can be expressed as

$$a_n^{m-1} J_n(k_{m-1} R_m) + b_n^{m-1} H_n^{(2)}(k_{m-1} R_m) = 0 \quad (20)$$

The reflection coefficient Γ_n^{m-1} is

$$\Gamma_n^{m-1} = \frac{b_n^{m-1}}{a_n^{m-1}} = -\frac{J_n(k_{m-1} R_m)}{H_n^{(2)}(k_{m-1} R_m)} \quad (21)$$

For a dielectric rod, there are no scattered fields inside the dielectric, which means $\mathbf{b}_m = \mathbf{0}$ in Eq. (9). Thus, the reflection coefficient Γ_n^{m-1} for a dielectric rod can be expressed as

$$\Gamma_n^{m-1} = \frac{b_n^{m-1}}{a_n^{m-1}} = S_{11,m-1}^n \quad (22)$$

$S_{11,m-1}^n$ is the n th element of the diagonal matrix $\mathbf{S}_{11,m-1}$.

Thus, reflection matrix $\mathbf{\Gamma}_{m-1}$, which is a $(2N+1) \times (2N+1)$ diagonal matrix consisting of Γ_n^{m-1} , can be defined to express the relationship between \mathbf{a}_{m-1} and \mathbf{b}_{m-1} :

$$\mathbf{b}_{m-1} = \mathbf{\Gamma}_{m-1} \mathbf{a}_{m-1} \quad (23)$$

2.3. Reflection Matrix of Multilayered Concentric Dielectric Rod

The reflection matrix $\mathbf{\Gamma}_0$ of the m -layer concentric dielectric rod can be obtained by iterative calculation. The reflection matrix $\mathbf{\Gamma}_{m-1}$ of the m th layer is shown in Section 2.2. In the $(m-1)$ th layer, the scattering equation is

$$\begin{bmatrix} \mathbf{b}_{m-2} \\ \mathbf{a}_{m-1} \end{bmatrix} = \begin{bmatrix} \mathbf{S}_{11,m-2} & \mathbf{S}_{12,m-2} \\ \mathbf{S}_{21,m-2} & \mathbf{S}_{22,m-2} \end{bmatrix} \begin{bmatrix} \mathbf{a}_{m-2} \\ \mathbf{b}_{m-1} \end{bmatrix} \quad (24)$$

Substituting Eq. (23) into Eq. (24) leads to

$$\mathbf{b}_{m-2} = \left(\mathbf{S}_{11,m-2} + \mathbf{S}_{12,m-2} (\mathbf{\Gamma}_{m-1}^{-1} - \mathbf{S}_{22,m-2})^{-1} \mathbf{S}_{21,m-2} \right) \mathbf{a}_{m-2} \quad (25)$$

From Eq. (25), the reflection matrix $\mathbf{\Gamma}_{m-2}$ of the $(m-1)$ th layer can be written as

$$\mathbf{\Gamma}_{m-2} = \begin{bmatrix} \mathbf{b}_{m-2} \\ \mathbf{a}_{m-2} \end{bmatrix} = \mathbf{S}_{11,m-2} + \mathbf{S}_{12,m-2} (\mathbf{\Gamma}_{m-1}^{-1} - \mathbf{S}_{22,m-2})^{-1} \mathbf{S}_{21,m-2} \quad (26)$$

Repeating the calculation process of Eqs. (24) and (25), the reflection matrix $\mathbf{\Gamma}_0$, as shown in Fig. 3, can be obtained by iterative calculation.

2.4. Reflection Matrix of Multilayered Eccentric Dielectric Rod

In Section 2.3, the cylindrical coordinate is set up at the center of the rod. For the eccentric dielectric rod, the center of each layer varies. The main issue to get the reflection matrix is to adjust the coefficients to fit the varying local coordinate.

For a m -layer eccentric dielectric rod, the local coordinates which are set up at the center of each layer are named as $x_i o_i y_i (i = 1, 2, \dots, m)$. In Section 2.1, the electric fields and magnetic fields are

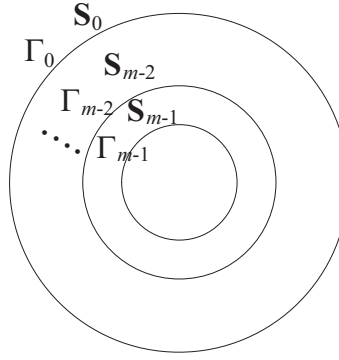


Figure 3. Reflection matrix of each layer.

expressed by the Bessel function and the Hankel function. When the local coordinate changes from $x_i o_i y_i$ to $x_j o_j y_j$, as shown in Fig. 4, the Bessel function and the Hankel function should be re-expressed by a transformation matrix \mathbf{T}_{ji} . According to the Bessel addition theorem, the transformation matrix can be written as

$$\mathbf{T}_{ji} = [\mathbf{T}_{ji}(\mathbf{m}, \mathbf{n})]_{(2N+1) \times (2N+1)} \quad (27)$$

for the Bessel function

$$T_{ji}(m, n) = J_{m-n}(k|\vec{\rho}_{ji}|)e^{-j(m-n)\phi_{ji}} \quad (28)$$

for the Hankel function

$$T_{ji}(m, n) = \begin{cases} J_{m-n}(k|\vec{\rho}_{ji}|)e^{-j(m-n)\phi_{ji}} & |\vec{\rho}_{ji}| < |\vec{\rho}_i| \\ J_{m-n}(k|\vec{\rho}_i|)e^{-j(m-n)\phi_{ji}} & |\vec{\rho}_{ji}| \geq |\vec{\rho}_i| \end{cases} \quad (29)$$

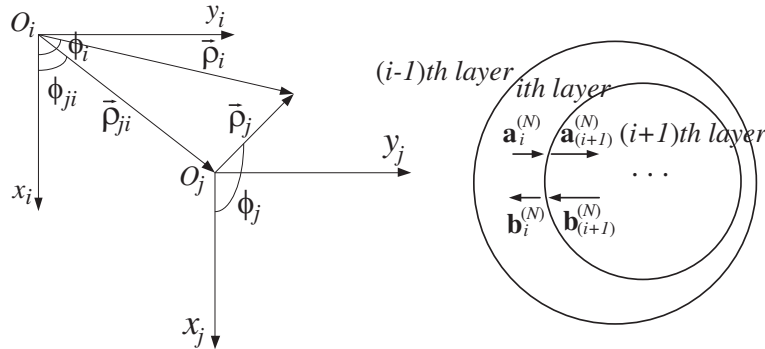


Figure 4. The transformation from coordinate $x_i o_i y_i$ to $x_j o_j y_j$.

In local cylindrical coordinate $x_i o_i y_i$, as discussed in Sections 2.2 and 2.3, the relationship between the incident and scattered fields in the i th layer can be expressed as

$$\mathbf{b}_i = \mathbf{\Gamma}_i \mathbf{a}_i \quad (30)$$

In the coordinate system $x_{i-1} o_{i-1} y_{i-1}$, the formula (30) needs to be written as Eqs. (31)–(33)

$$\mathbf{T}_{(i-1)i} \mathbf{b}_i = \mathbf{\Gamma}_i \mathbf{T}_{(i-1)i} \mathbf{a}_i \quad (31)$$

$$\mathbf{b}_i = \mathbf{T}_{(i-1)i}^{-1} \mathbf{\Gamma}_i \mathbf{T}_{(i-1)i} \mathbf{a}_i = \mathbf{T}_{i(i-1)} \mathbf{\Gamma}_i \mathbf{T}_{(i-1)i} \mathbf{a}_i \quad (32)$$

$$\mathbf{\Gamma}'_i = \mathbf{T}_{i(i-1)} \mathbf{\Gamma}_i \mathbf{T}_{(i-1)i} \quad (33)$$

$\mathbf{\Gamma}_i$ means the relationship between \mathbf{a}_i and \mathbf{b}_i in $x_i o_i y_i$, and $\mathbf{\Gamma}'_i$ means the relationship between \mathbf{a}_i and \mathbf{b}_i in $x_{i-1} o_{i-1} y_{i-1}$.

Substituting Eq. (33) into Eq. (26), replacing the Γ_i with the Γ'_i , the reflection matrix of the $(i-1)$ th layer in the coordinate system $x_{i-1}o_{i-1}y_{i-1}$ can be obtained.

$$\Gamma_{i-1} = \mathbf{S}_{11,i-1} + \mathbf{S}_{12,i-1} (\Gamma'_i - \mathbf{S}_{22,i-1})^{-1} \mathbf{S}_{21,i-1} \quad (34)$$

Repeating formulas (26)–(34), the reflection matrix Γ_0 of the eccentric rod can be calculated layer by layer.

3. RADIAL SCATTERING MATRIX FOR POWER/GROUND PLANES LOADED WITH REFLECTION MATRIX OF MULTILAYERED DIELECTRIC RODS

In this section, the multilayered rod forest is considered, imitating the model in [14] as an EBG structure. There are P multilayered dielectric rods and Q vias located in the plate pair. The dielectric rods are viewed as loaded ports and the vias are viewed as source ports. The locations of those radial ports are presented in global coordinate by

$$\vec{\rho}_i = (\rho_i, \varphi_i), \quad i = 1, 2, 3, \dots, P, P+1, \dots, P+Q$$

The point in the local coordinate which is set up at the center of each radial port is presented by $\vec{\rho}^i = (\rho^i, \varphi^i)$ as shown in Fig. 5. Generally, the superscript means the local coordinate and the subscript means the global coordinate.

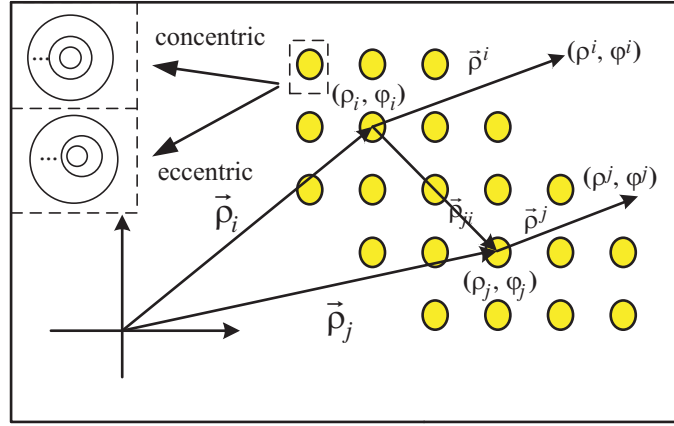


Figure 5. Top view of rod forest and the global or local coordinate system.

In the rod forest, the scattered cylindrical harmonics from the i th port will illuminate the j th port. It means that the scattered cylindrical harmonics \mathbf{b}_i in coordinate $x_i o_i y_i$ is the incident cylindrical harmonics \mathbf{a}_j in coordinate $x_j o_j y_j$. As discussed in Section 2, the transformation matrix \mathbf{T}_{ji} is applied to describe this phenomenon.

$$\mathbf{a}_j = \mathbf{T}_{ji} \mathbf{b}_i \quad (35)$$

where \mathbf{T}_{ji} is a $(2N+1) \times (2N+1)$ matrix, and it can be obtained by Eqs. (27)–(29) for a regular infinite plate pair.

For P loaded ports and Q source ports, the combined matrix of the addition theorem coefficients can be expressed as

$$\mathbf{T} = \begin{bmatrix} \mathbf{T}_{11} & \mathbf{T}_{12} & \cdots & \mathbf{T}_{1(P+Q)} \\ \mathbf{T}_{21} & \mathbf{T}_{22} & \cdots & \mathbf{T}_{2(P+Q)} \\ \vdots & \ddots & \ddots & \vdots \\ \mathbf{T}_{(P+Q)1} & \mathbf{T}_{(P+Q)2} & \cdots & \mathbf{T}_{(P+Q)(P+Q)} \end{bmatrix} \quad (36)$$

To distinguish the source ports and loaded ports, the matrix \mathbf{T} is divided into four block matrix as:

$$\begin{bmatrix} \mathbf{a}_l \\ \mathbf{a}_s \end{bmatrix} = \begin{bmatrix} \mathbf{T}_{ll} & \mathbf{T}_{ls} \\ \mathbf{T}_{sl} & \mathbf{T}_{ss} \end{bmatrix} \begin{bmatrix} \mathbf{b}_l \\ \mathbf{b}_s \end{bmatrix} \quad (37)$$

where subscript s and l means the source ports and loaded ports, respectively. As described in Section 2, the block matrix \mathbf{a}_l and \mathbf{b}_l can be written as

$$\mathbf{b}_l = \Gamma_l \mathbf{a}_l \tag{38}$$

And from (37), \mathbf{a}_l can be expressed as

$$\mathbf{a}_l = \mathbf{T}_{ll} \mathbf{b}_l + \mathbf{T}_{ls} \mathbf{b}_s \tag{39}$$

Substituting Eq. (39) to Eq. (38), the \mathbf{b}_l and \mathbf{a}_s can be expressed as

$$\mathbf{b}_l = (\mathbf{I} - \Gamma_l \mathbf{T}_{ll})^{-1} \Gamma_l \mathbf{T}_{ls} \mathbf{b}_s \tag{40}$$

$$\mathbf{a}_s = [\mathbf{T}_{ss} + \mathbf{T}_{sl} (\mathbf{I} - \Gamma_l \mathbf{T}_{ll})^{-1} \Gamma_l \mathbf{T}_{ls}] \mathbf{b}_s \tag{41}$$

Through Eq. (41), the coupling between two source ports among dielectric rod forest can be calculated.

4. NUMERICAL EXAMPLES AND DISCUSSIONS

Several examples are provided to validate the accuracy and the efficiency of the proposed method in this section. The simulation results are conducted by a full-wave field simulator CST based on the finite integration technique (FIT) on a machine with 2 GHz CPU and 32 GB RAM.

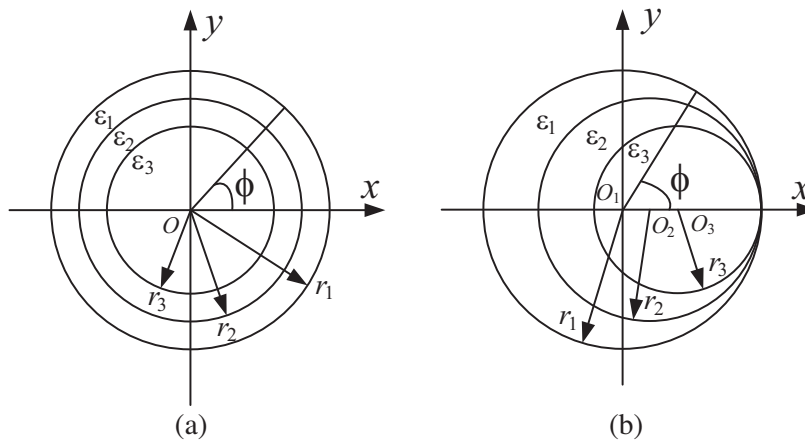


Figure 6. Top view and the parameters. (a) Concentric rod. (b) Eccentric rod.

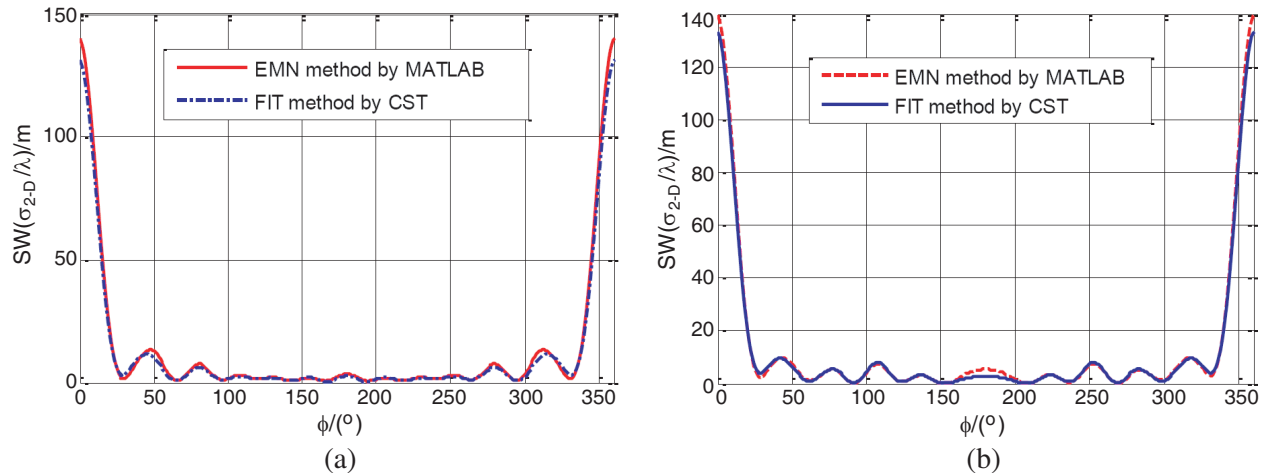


Figure 7. SW of the multilayered rod. (a) Concentric rod. (b) Eccentric rod.

Figure 6 shows a three-layer concentric dielectric rod and a three-layer eccentric dielectric rod. The relative permittivity $\varepsilon_1, \varepsilon_2, \varepsilon_3$ are 2, 3, 4 and radii r_1, r_2, r_3 are 0.1 m, 0.08 m, 0.06 m, respectively. In Fig. 6(b), the centers of these three rods O_1, O_2, O_3 are $(0, 0), (0.02, 0), (0.04, 0)$, respectively. ϕ is the angle between the observation point and the $+x$ axis. The source is a plane wave traveling in the $+x$ direction. The truncation number N , which is described below (4), is set as 25. The scattering width (SW) at 3 GHz is applied to demonstrate the accuracy of the EMN method proposed in this article. The simulation results match well with the EMN results as shown in Fig. 7.

The second example is a photonic crystal power/ground layer (PCPL) with multilayered dielectric rod forest. As shown in Fig. 8, the dimensions of the PCPL structure are 62.5×100 mm, and the structure is divided into 40 units on average. There are 40 two-layer dielectric rods embedded on the lossless dielectric substrate whose dielectric constant ε_0 is 2.33. The radii of those two-layer concentric rods are $r_1 = 2$ mm, $r_2 = 1$ mm, and the relative dielectric constant of the lossless rods are $\varepsilon_1 = 102$, $\varepsilon_2 = 4.4$. The rods have the same height with the parallel plate separation. The power/ground metal plates are modeled as PEC with a thickness of 0.03556 mm. The origin of the Cartesian coordinate is located at the bottom left corner of the parallel plates, and the two vias or source ports are located at $P1$ (12.5 mm, 25 mm) and $P2$ (25 mm, 46.5 mm).

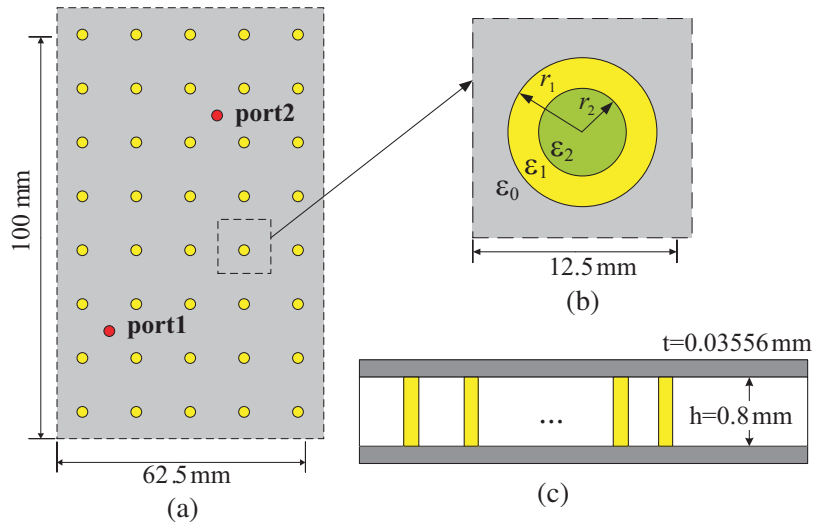


Figure 8. The structure of PCPL. (a) Top view. (b) Partial enlarged drawing of one unit. (c) Cross-section view.

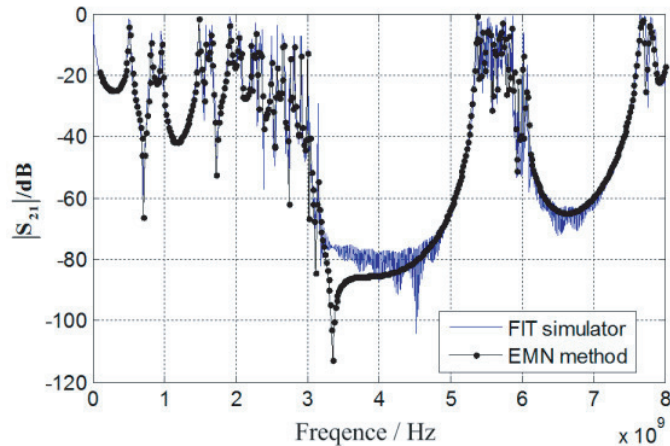


Figure 9. Comparison of $|S_{21}|$ by EMN method and FIT simulator.

The coupling between the source ports can be described by S_{21} parameter. Fig. 9 shows the magnitude of S_{21} by FIT simulator CST and the numerical results of EMN method. Great agreements can be seen between these two methods. There are two stopbands, from 3 to 5.5 GHz and 6 to 7.5 GHz. The main discrepancies in the stopband from 3 to 5.5 GHz are caused by the spurious rapid resonances in the FIT simulator and the drawback of the time-domain solver for high-Q resonators formed by PCPL. Additional, in this example, it took about 1 minute by MATLAB code with the EMN method, while FIT simulator spent more than 20 hours.

5. CONCLUSION

Equivalent microwave network method (EMN) is proposed in this article to analyze the concentric and eccentric multilayered dielectric rods. The reflection matrix and transformation matrix are introduced into the calculation. The reflection matrix of multilayered dielectric rod is calculated and loaded to radial scattering matrix to analyze a novel EBG structure. All the numeric calculation results match well with the full-wave simulations and the EMN method is efficient and flexible for modeling PCPL structure.

REFERENCES

1. Oo, Z. Z., E. X. Liu, E. P. Li, and Y. J. Zhang, "Computing the RCS of dielectric coated objects using multilevel fast multipole algorithm: Impedance boundary condition approach," *International Conference on Computational Electromagnetics and ITS Applications, 2004, Proceedings, ICCEA*, 100–103, 2004.
2. Lee, S. C., "Scattering by closely spaced parallel nonhomogeneous cylinders in an absorbing medium," *Journal of the Optical Society of America A*, Vol. 28, No. 9, 1812–1819, 2011.
3. Leviatan, Y. and A. Boag, "Analysis of electromagnetic scattering from dielectrically coated conducting cylinders using a multifilament current model," *IEEE Transactions on Antennas & Propagation*, Vol. 35, No. 11, 1119–1127, 1987.
4. Barabls, M., "Scattering of a plane wave by a radially stratified tilted cylinder," *Journal of the Optical Society of America A*, Vol. 4, No. 12, 2240–2248, 1987.
5. Lee, S. C. and J. A. Grzesik, "Light scattering by closely spaced parallel cylinders embedded in a semi-infinite dielectric medium," *Journal of the Optical Society of America A*, Vol. 15, No. 1, 163–173, 1998.
6. Yasumoto, K., V. Jandieri, and B. Gupta, "Electromagnetic scattering by cylindrical arrays of circular rods," *IEEE Transactions on Antennas & Propagation*, Vol. 59, No. 6, 312–315, 2009.
7. Kishk, A. A., R. P. Parrikar, and A. Z. Elsherbeni, "Electromagnetic scattering from an eccentric multilayered circular cylinder," *IEEE Transactions on Antennas and Propagation*, Vol. 40, No. 3, 295–303, 1992.
8. Stratigaki, L. G., "Scattering from a dielectric cylinder with multiple eccentric cylindrical dielectric inclusions," *IEE Proceedings — Microwaves Antennas and Propagation*, Vol. 143, No. 6, 505–511, 1996.
9. Ioannidou, M. P., K. D. Kapsalas, and D. P. Chrissoulidis, "Electromagnetic-wave scattering by an eccentrically stratified, dielectric cylinder with multiple, eccentrically stratified, cylindrical, dielectric inclusions," *Journal of Electromagnetic Waves and Applications*, Vol. 18, No. 4, 495–516, 2004.
10. Jarem, J. M., "Rigorous coupled wave analysis of bipolar cylindrical systems: Scattering from inhomogeneous dielectric material, eccentric, composite circular cylinders," *Progress In Electromagnetics Research*, Vol. 18, No. 1, 181–237, 2003.
11. Jarem, J. M., "Rigorous coupled wave theory of anisotropic, azimuthally-inhomogeneous cylindrical systems," *Journal of Electromagnetic Waves and Applications*, Vol. 19, No. 7, 911–912, 2012.
12. Jarem, J. M., "Rigorous coupled wave analysis of radially and azimuthally-inhomogeneous, elliptical, cylindrical systems," *Progress In Electromagnetics Research*, Vol. 15, 89–115, 2001.

13. Zhang, Y. J. and J. Fan, "A generalized multiple scattering method for dense vias with axially anisotropic modes in an arbitrarily shaped plate pair," *IEEE Transactions on Microwave Theory and Techniques*, Vol. 60, No. 7, 2035–2045, 2012.
14. Tian, X., Y. J. Zhang, D. Liu, and L. Gui, "Efficient analysis of power/ground planes loaded with dielectric rods and decoupling capacitors by extended generalized multiple scattering method," *IEEE Transactions on Electromagnetic Compatibility*, Vol. 57, No. 1, 135–144, 2015.
15. Balanis, C. A. and J. Wiley, *Advanced Engineering Electromagnetics*, Wiley & Sons, Canada, 1989.